


Plaquette valence bond solid to antiferromagnet transition and deconfined quantum critical point of the Shastry-Sutherland model

Ning Xi,^{1,*}† Hongyu Chen^{1,*}‡, Z. Y. Xie^{1,2,‡} and Rong Yu^{1,2,§}

¹Department of Physics and Beijing Key Laboratory of Opto-electronic Functional Materials and Micro-nano Devices, Renmin University of China, Beijing 100872, China

²Key Laboratory of Quantum State Construction and Manipulation (Ministry of Education), Renmin University of China, Beijing 100872, China

 (Received 20 November 2021; revised 19 January 2023; accepted 22 June 2023; published 29 June 2023)

We study the ground-state phase diagram of the Shastry-Sutherland model by using a variational optimization of the infinite tensor network states, and identify a weakly first-order transition between the plaquette valence bond solid and the antiferromagnetic states. The full plaquette state is found to strongly compete with the empty plaquette ground state, and can be stabilized as the ground state when a staggered ring-exchange interaction preserving the Shastry-Sutherland lattice symmetry is introduced. We propose the triple point where the full plaquette, empty plaquette, and antiferromagnetic phases meet as a deconfined quantum critical point (DQCP). The analysis of susceptibilities provides evidence of an emergent SO(5) symmetry at this point. These results shed light on the study of DQCP in quantum magnets and provide a way to understand the proximate DQCP signatures in recent experiments on SrCu₂(BO₃)₂.

DOI: [10.1103/PhysRevB.107.L220408](https://doi.org/10.1103/PhysRevB.107.L220408)

Introduction. Enhanced quantum fluctuations in a frustrated spin system can give rise to exotic quantum phases, including the quantum spin liquid (QSL), valence bond solid (VBS), and spin nematicity [1–6]. The nature of these novel quantum phases and related quantum phase transitions has been extensively studied. Though most transitions can be described within the standard Ginzburg-Landau-Wilson (GLW) paradigm, it has been proposed that the transition between a VBS and an antiferromagnetic (AFM) phase is beyond the GLW scenario, e.g., via a deconfined quantum critical point (DQCP) [7]. At this point, deconfined fractionalized excitations emerge, and the enhanced symmetry allows a continuous rotation between the two distinct order parameters. This new scenario has inspired extensive studies [8–12], but it is still challenging to realize a DQCP in two-dimensional (2D) frustrated spin systems, and the nature of this critical point needs to be explored.

The Shastry-Sutherland (SS) model [13] is an ideal frustrated spin model for studying the VBS-AFM transition [14–21]. It is defined on the SS lattice as sketched in Fig. 1(a), and the Hamiltonian reads

$$\hat{H}_{SS} = J \sum_{\langle i,j \rangle} \mathbf{S}_i \cdot \mathbf{S}_j + J' \sum_{\langle\langle i,j \rangle\rangle} \mathbf{S}_i \cdot \mathbf{S}_j, \quad (1)$$

where \mathbf{S}_i is an $S = 1/2$ spin on site i , and J and J' refer to the nearest- and next-nearest-neighbor couplings, respectively. As

demonstrated in Fig. 1(c), the ground state is found to be a product of dimer singlets (DSs) along the diagonal directions for $J/J' \lesssim 0.68$ [14,17]. For $J/J' \gtrsim 0.68$, the ground state first changes to a plaquette VBS, then to a Néel AFM state with increasing J/J' [14,17,19]. A first-order transition between the DS and plaquette phases has been verified by various numerical results. However, the understanding of the plaquette-AFM transition remains controversial: A series expansion study [14] found a second-order transition, while an infinite projected entangled pair state (iPEPS) tensor network calculation [17] showed it to be weakly first order. A recent density matrix renormalization group (DMRG) study [19] proposed the transition is through a DQCP with an emergent $O(4)$ symmetry, but another DMRG work [20] suggested a gapless QSL settles in between the plaquette and AFM phases.

The SS model is believed to properly describe the quantum magnetism of the quasi-2D material SrCu₂(BO₃)₂ [14,22,23]. Evidence of the evolution from the DS to a plaquette then to an AFM state under pressure has been cumulated via inelastic neutron scattering (INS) [24], nuclear magnetic resonance (NMR) [25,26], Raman scattering [27], and specific heat [28,29] measurements. Some experimental results imply the intermediate plaquette ground state has a full plaquette (FPL) pattern, that is, the local singlet spans on the plaquette with a diagonal J_2 bond [24,27,30]. However, numerical calculations on the SS model [17–20] suggest an empty plaquette (EPL) ground state [Fig. 1(c)]. Though it was shown theoretically that the FPL can be stabilized as the ground state when the SS lattice symmetry is broken [18], the suggested symmetry breaking has not been observed. Moreover, the symmetry breaking is incompatible with the DQCP scenario, which is suggested by recent NMR measurements [30]. Therefore, the nature of the PL state is still an open issue crucial to the study of DQCP in SS systems.

*These authors contributed equally to this work.

†Present address: CAS Key Laboratory of Theoretical Physics, Institute of Theoretical Physics, Chinese Academy of Sciences, Beijing 100190, China.

‡qingtaoxie@ruc.edu.cn

§rong.yu@ruc.edu.cn

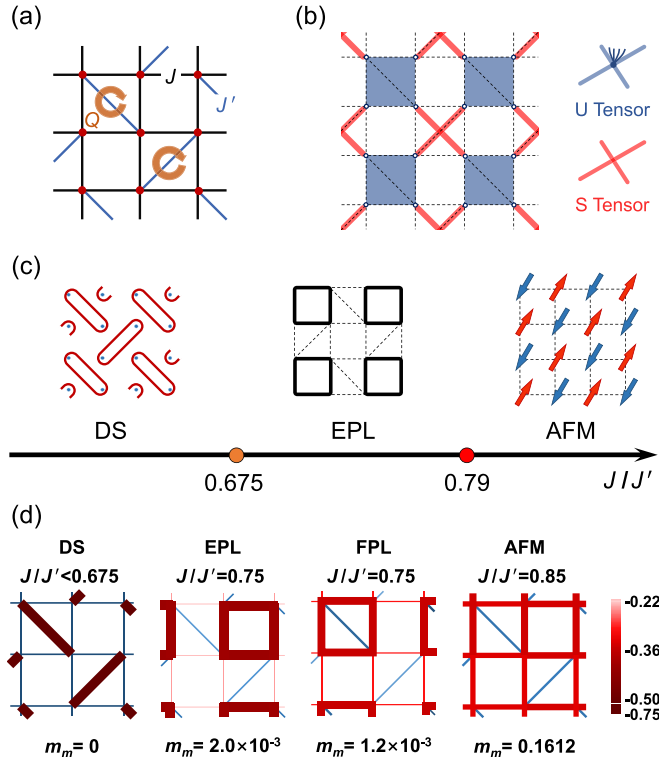


FIG. 1. (a) Sketch of the generalized SS model. J and J' refers to the nearest- and next-nearest-neighbor Heisenberg couplings. Q refers to the staggered ring-exchange interaction \hat{H}_Q . (b) The 16-PESS setup on the SS lattice. The tensors are placed at the plaquette within the J' coupling. Each U tensor (blue) consists of four physical spin indices and four auxiliary ones, while an S tensor contains four auxiliary indices only. (c) The ground-state phase diagram of the SS model. DS, EPL, and AFM refer to dimer singlet, empty plaquette, and antiferromagnetic phases, respectively. Both the DS-EPL and EPL-AFM transitions are found to be first order. (d) Typical configurations, corresponding spin-spin correlations, and magnetic order parameters of the DS, EPL, FPL, and AFM states in the calculation. The EPL and FPL have distinct characters of symmetry breaking.

In this Letter, we investigate the ground-state phase diagram of the SS model by using a variational optimization of the infinite tensor network states with the projected entangled simplex state (PESS) construction. Our calculation clarifies the intermediate phase to be an EPL, and our results evidence a weakly first-order EPL-AFM transition at $J/J' \approx 0.79$, without an intervening QSL. Nevertheless, the FPL state is found to be intimately competing with the EPL ground state, with an energy difference less than $10^{-4}J$. By including a staggered ring-exchange interaction as a symmetry-preserving perturbation, we show the ground state can change from the EPL to FPL. In light of this observation, we establish a global phase diagram of this generalized SS model, and propose the triple point among the FPL, EPL, and AFM phases as a DQCP. By analyzing susceptibilities associated with order parameters, we provide evidence of an emergent $SO(5)$ symmetry at the DQCP. These results reveal the unusual physics of DQCP in SS model and related experimental systems.

Model and method. We consider the ground states of the SS model defined in Eq. (1). To investigate the stability of

the EPL vs FPL, we also consider a generalized SS model by including a staggered ring-exchange interaction \hat{H}_Q within neighbor spins of a plaquette with J' coupling [see the inset of Fig. 1(a)]:

$$\hat{H}_Q = -Q \sum_{ijkl \in \square} (\mathbf{S}_i \cdot \mathbf{S}_j)(\mathbf{S}_k \cdot \mathbf{S}_l) + (\mathbf{S}_i \cdot \mathbf{S}_k)(\mathbf{S}_j \cdot \mathbf{S}_l). \quad (2)$$

The ground states are obtained by using the variational optimization of the 16-PESS tensor network states [31]. The PESS construction of the tensor network states has been shown to give an excellent description of the ground state of frustrated spin systems [32,33]. On the SS lattice, the 16-PESS is constructed with U and S tensors, as illustrated in Fig. 1(b). A projection tensor U is defined on a plaquette with the J' interaction, and carries the four spins in this plaquette. Four adjacent U tensors are then connected by an entangled simplex tensor S . The S tensor is introduced to describe the entanglement among the spin clusters but itself does not carry any physical spin degree of freedom. In this work, we find a 2×2 unit cell with one independent pair of U and S tensors is sufficient to characterize the ground state. The calculation is performed in an infinitely large system by employing translational symmetry.

To determine the ground states, we adopt an advanced variational optimization method to globally minimize the ground-state energy $\langle \psi | \hat{H} | \psi \rangle / \langle \psi | \psi \rangle$. We are inspired by differentiable programming [34–36], which can be effectively combined with other well-developed techniques [37–41]. To be specific, the state for optimization is initialized from an arbitrary state or an approximately converged state obtained from (imaginary) time evolution [32,37,39,41]. Then we use the corner transfer matrix renormalization group (CTMRG) method [38,42] to contract the infinite network and get the approximate environment of the local tensors. After that, we use the quasi-Newton limited memory Broyden-Fletcher-Goldfarb-Shanno (L-BFGS) algorithm to minimize the energy density, which can be effectively implemented by the ZYGOTE package [43]. The automatic differentiation provides a global optimization strategy of the ground state, and is more reliable than local optimization approaches, especially for critical systems where many competing states exist. Technical details and benchmarking of this combination of 16-PESS ansatz and the automatic differentiation can be found in the Supplemental Material (SM) [31].

Weakly first-order plaquette-AFM transition. For the SS model, as demonstrated in Fig. 1(c), we find the ground state is the DS for $J/J' < 0.675$, consistent with previous results [14,17,19]. Increasing J/J' , the ground state first changes to the EPL, then to the AFM at $J/J' \approx 0.79$. To examine the plaquette-AFM transition, we calculate the ground-state energy E and its derivative dE/dJ . The results for $D = 5$ are shown in Fig. 2(a) and 2(b), respectively. Though E varies smoothly across the transition, dE/dJ shows a small discontinuity at $J/J' \approx 0.78$, featuring a weakly first-order transition. We further calculated the order parameters m_m and m_p of the AFM and plaquette phases, respectively: $m_m = \sqrt{\langle m_m^x \rangle^2 + \langle m_m^y \rangle^2 + \langle m_m^z \rangle^2}$, and $m_p = |\sum_{(ij) \in \square_A} \langle \mathbf{S}_i \cdot \mathbf{S}_j \rangle - \sum_{(ij) \in \square_B} \langle \mathbf{S}_i \cdot \mathbf{S}_j \rangle|$. Here, $\langle m_m^\alpha \rangle = \frac{1}{N} \sum_i \langle e^{i\mathbf{Q} \cdot \mathbf{r}_i} S_{r_i}^\alpha \rangle_{r_i}$ for $\alpha = x, y, z$, $\mathbf{Q} = (\pi, \pi)$, and $\square_{A/B}$ label

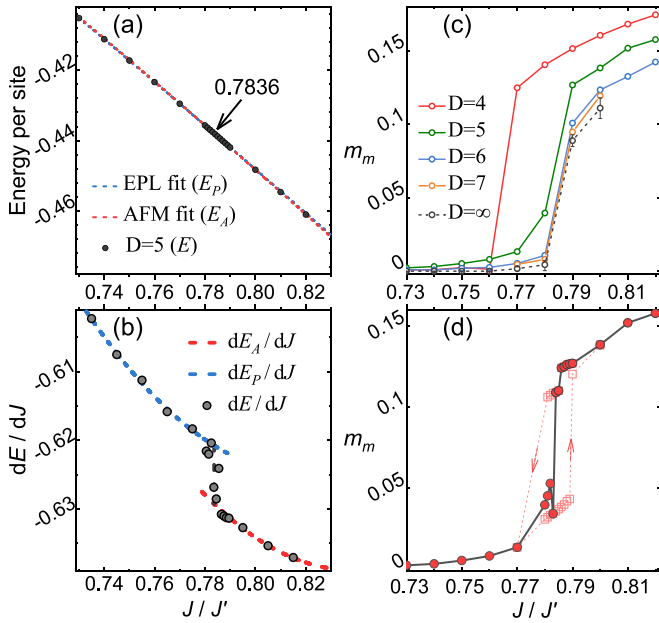


FIG. 2. Ground-state properties of SS model. (a) The ground-state energy per site with J/J' at $D=5$. The blue (red) dashed line is the fitted energy E_A (E_P) in the AFM (plaquette) phase (see text). (b) The first-order derivative dE/dJ with J/J' shows a clear discontinuity at the plaquette-AFM transition. (c) Finite- D analysis and the extrapolated m_m with J/J' . (d) The staggered magnetization m_m with J/J' for $D=5$. Solid circles show m_m values of the lowest-energy configurations, while open squares are obtained with biased configurations (see text) and exhibit a clear hysteresis loop.

the two inequivalent empty plaquettes. As shown by the solid curves with solid symbols in Fig. 2(d), m_m exhibits a small but finite abrupt jump near $J/J' \approx 0.78$, consistent with the dE/dJ result. As shown in Fig. 2(c), the jump of m_m is seen for all the finite D values we studied, and is robust even in the large- D limit after proper extrapolation. To further verify the first-order nature of the transition, we first stabilize the plaquette (AFM) state from our optimization at a J/J' ratio far from the transition, then slowly increase (decrease) J/J' . At each step, we take the converged state obtained from the last step as the initial state for optimization. We repeat this procedure until the system is driven through the transition to the AFM (plaquette) phase. As shown by the dashed curves with open symbols in Fig. 2(d), m_m exhibits a clear hysteresis loop, indicating the existence of metastable states, which is a prominent signature of a first-order transition. Similar behavior of m_p confirms the first-order transition behavior [31]. The transition point is determined to be $(J/J')_c \approx 0.79$ in the large- D limit from the crossing point of the fitted energies in the plaquette and AFM phase. Details of the fitting and extrapolation procedures are presented in SM [31].

Nature of the plaquette ground state. In the parameter regime $0.68 \lesssim J/J' \lesssim 0.79$, we are able to stabilize both two plaquette states in the calculation [see Fig. 1(d)], and we find the energy of the EPL state is always lower than that of the FPL. Interestingly, near the transition point, the energies of these two states become very close, as shown in Fig. 3(a). In the large- D limit, the energy difference is less than $10^{-4}J$.

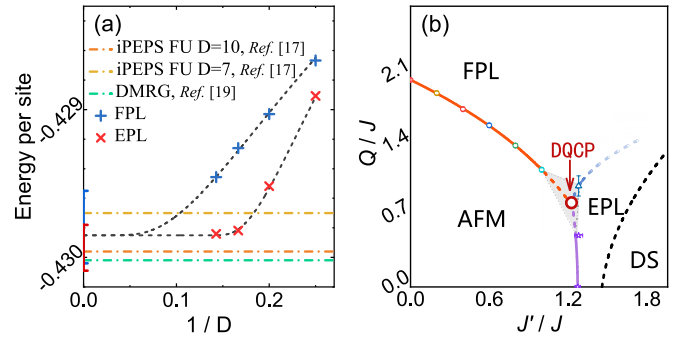


FIG. 3. (a) Energies of EPL and FPL states vs $1/D$ at $J/J' = 0.77$. The horizontal dashed-dotted lines show the plaquette ground-state energies in iPEPS [17] and DMRG [19] studies for comparison. (b) Ground-state phase diagram of the generalized SS model that preserves the SS lattice symmetry. Besides the DS phase (not shown), EPL, FPL, and AFM phases are stabilized as the ground states. Symbols show the transition points and the lines are guides to the eyes. The triple point of the EPL, FPL, and AFM phases is proposed as a DQCP (see text).

Such a small energy difference is about the same order as the one between the EPL and AFM states near the transition (see Fig. S4 of SM [31]). This implies that the FPL state, though never favored as the ground state, emerges as a low-lying competing state near the plaquette-AFM transition. Actually, besides the FPL, we can also stabilize other metastable states with competitive energies near the transition. The emergence of these metastable states suggests enhanced low-energy fluctuations, and is consistent with the weakly first-order transition we found.

Global phase diagram and possible DQCP. The quasidegeneracy between the EPL and FPL states prompts that an FPL ground state can be stabilized nearby if we consider a global phase diagram with an extra tuning parameter. Such a global phase diagram would help solving the paradox on the nature of the plaquette ground state between theory and experiments. A previous theoretical work [18] found a quasi-one-dimensional singlet phase adiabatically connected to the FPL when the symmetry between the two diagonal J' bonds is broken. However, the orthogonal lattice distortion accounting for this symmetry breaking has not been verified experimentally. For example, a recent NMR study on $\text{SrCu}_2(\text{BO}_3)_2$ claiming proximate DQCP between the FPL and AFM phases [30] shows no signature of the orthogonal lattice distortion. To reconcile the discrepancy between theory and experiments, here we adopt a different strategy: Tune the stability of the EPL and FPL phases without breaking the SS lattice symmetry. For this purpose, we generalize the SS model by including a ring-exchange-like interaction.

The model Hamiltonian reads $\hat{H} = \hat{H}_{\text{SS}} + \hat{H}_{\text{Q}}$, where \hat{H}_{SS} and \hat{H}_{Q} are given in Eqs. (1) and (2), respectively. The global phase diagram in the J - Q plane is illustrated in Fig. 3(b). It is shown that the EPL, FPL, and AFM states span a broad regime, and the ring-exchange term \hat{H}_{Q} favors the FPL ground state over the EPL state. We find the FPL-AFM transition is also weakly first order, as evidenced by the discontinuity of the ground-state energy derivative dE/dQ

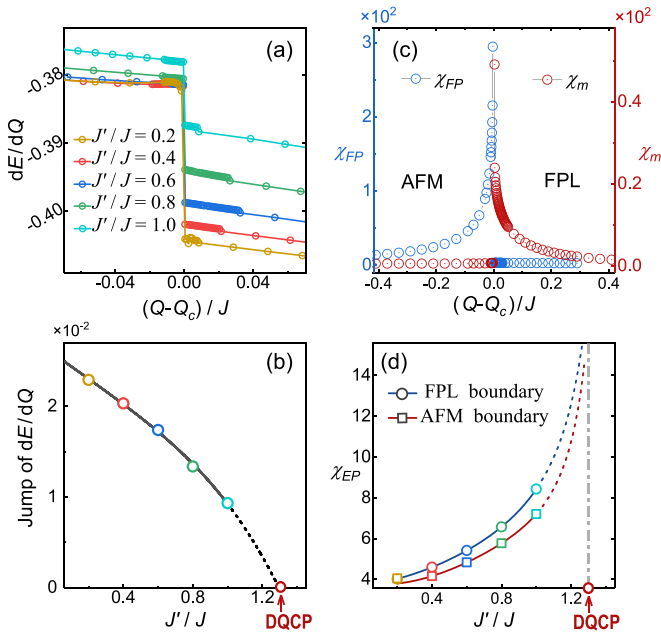


FIG. 4. Ground-state properties of generalized SS model. (a) The derivative of the ground-state energy dE/dQ with $(Q - Q_c)/J$, where Q_c is the FPL-AFM transition point. The jump of dE/dQ at $Q = Q_c$ indicates a first-order transition. (b) The discontinuity of dE/dQ at $Q = Q_c$ vs J'/J . The discontinuity vanishes when approaching the triple point, implying it is a DQCP. (c) The FPL susceptibility χ_{FP} and AFM susceptibility χ_m vs $(Q - Q_c)/J$ at $J'/J = 0.6$. (d) The EPL susceptibility χ_{EP} vs J'/J when approaching the triple point. χ_{EP} is calculated slightly away from the transition point Q_c in the AFM and FPL phases, respectively.

[Figs. 4(a) and 4(b)]. Remarkably, the discontinuity of the energy derivative reduces along the FPL-AFM transition trajectory toward the triple point among the EPL, FPL, and AFM phases. It is fully suppressed when extrapolating to the triple point, as shown in Fig. 4(b). This implies that the triple point is a quantum critical point. Note that our model preserves the SS lattice symmetry and the three phases break distinct symmetries. A conventional continuous transition is then prohibited within the LGW paradigm. We therefore propose this point as a DQCP.

The EPL and FPL states break different Z_2 lattice symmetries, and their order parameters can be combined to a complex (two-component) monopole operator [19]. Further taking the three-component spin order parameter of the AFM phase, this infers an enlarged $SO(5)$ symmetry [from $SO(3) \times Z_2 \times Z_2$] at the proposed DQCP. To examine the exact emergent symmetry at this point, we calculate the susceptibilities associated with the AFM, FPL, and EPL order parameters, χ_m , χ_{FP} , and χ_{EP} , respectively. For a conventional first-order transition, the two ordered phases are not related by any symmetry, so the susceptibility is expected to be finite in each phase, and experiences a jump across the transition. But the enhanced symmetry allows a continuous rotation between order parameters in different phases and causes additional gapless excitation modes, which are signaled by the divergence of order-parameter susceptibilities. We first study the first-order FPL-AFM transition. As shown in Fig. 4(c), for the transition

at $J'/J = 0.6$, χ_m tends to diverge when approaching to the transition point Q_c from the FPL phase, and vice versa for χ_{FP} . This divergent behavior indicates that the AFM and FPL order-parameter fluctuations are combined to a new excitation mode at the transition point, which contributes as an emergent Goldstone mode in addition to those stabilized in the AFM phase. This emergent Goldstone mode evidences an enhanced symmetry from $SO(3) \times Z_2$ to $O(4)$. We find this $O(4)$ symmetry emerges along the entire FPL-AFM transition trajectory, despite the first-order nature of the transition. Note that this symmetry is also found in a related J - Q model [45]. We then examine the behavior of χ_{EP} along the FPL-AFM transition line toward the triple point. To obtain the asymptotic behavior and avoid complexity caused by the first-order transition, we calculate χ_{EP} slightly away from Q_c in the FPL and AFM phases, respectively. As shown in Fig. 4(d), χ_{EP} increases rapidly with J'/J in either phase, suggesting a divergent behavior approaching the triple point. A divergent susceptibility indicates the existence of a soft mode, and the number of the soft modes is associated with the number of components N of the emergent $O(N)$ symmetry. Therefore, the simultaneous divergence of all order-parameter susceptibilities indicates the DQCP at the triple point has an enlarged $SO(5)$ symmetry.

Discussions and conclusion. As mentioned in the Introduction, the nature of the transition between the plaquette and AFM phases is under active debate. To address this issue numerically, it is important to accurately determine the ground-state energy. In our calculations, the ground state converges quickly with increasing D . Compared to other numerical methods, as shown in Fig. 3(a), the energy of the EPL state at $D = 6$ in our calculation is lower than that of a previous iPEPS work [17] for $D = 7$, and close to the $D = 10$ result and a DMRG one [19]. For the AFM state (see Fig. S5 of SM [31]) the energy at $D = 6$ in our work is lower than those of DMRG [20] and series expansion results [14].

The discontinuities of dE/dJ and m_m , as well as the hysteresis loop, unambiguously show a first-order EPL-AFM transition in the SS model, and rule out a continuous transition [19] or an intervening QSL phase [20]. The extrapolated transition points from different estimates are converged in our calculation. This suggests that a QSL regime [20], even if exists, should be very narrow in the parameter space. Our results also shed light on the VBS-AFM transitions in the square lattice J_1 - J_2 and checkerboard (CB) models [46–51], as both SS and CB models can be realized by depleting the J_2 bonds from the J_1 - J_2 model. In the CB model, the full and empty plaquettes have a more significant energy difference. We then expect the VBS-AFM transition there to be stronger first order. In the J_1 - J_2 model, however, the VBS-AFM transition should be weaker, or could even be intervened by a QSL, because the frustration is not released by depleting the J_2 bonds.

Here, we show a ring-exchange interaction, likely existing in $\text{SrCu}_2(\text{BO}_3)_2$, helps realize a DQCP [30]. Actually our argument for the DQCP is generic: This intriguing physics applies to any perturbation that preserves the SS lattice symmetry and can tune the ground state between EPL and FPL. Note that a DQCP does not exist in models breaking the SS lattice symmetry [18].

Our proposal of a DQCP with an emergent $SO(5)$ symmetry obviously differs from other theoretical suggestions in the SS model [19,20], in which the DQCP possesses an $O(4)$ symmetry. The different symmetry reflects an important difference in the structure of topological defects, whose proliferation causes deconfinement of spinons. For example, as in the columnar VBS phase [7], a topological defect carrying a spinon in the plaquette phase demands both EPL and FPL domains, and necessarily restores the $Z_2 \times Z_2$ symmetry. On the SS lattice, this can only happen when the EPL and FPL are degenerate, e.g., along the EPL-FPL transition line. The topological defects proliferate approaching the triple point (DQCP), where the symmetry is enlarged from $SO(3) \times Z_2 \times Z_2$ to $SO(5)$. On the other hand, for a DQCP with an $O(4)$ symmetry, the associated topological defect in the plaquette phase would carry multiple spinons, causing a very different low-energy spin excitation spectrum near the DQCP.

Our results provide a way to understand the proximate DQCP signatures in a recent experiment [30]. The DQCP stabilized in our model serves as an anchoring point for the proximate DQCP behavior observed experimentally. It has been shown that the $SO(5)$ DQCP causes a large anomalous dimension $\eta \approx 0.26$ [10], which naturally accounts for the observed $\eta \sim 0.2$ at the VBS-AFM transition in recent NMR measurements [30]. Moreover, our finding of the divergent

susceptibilities gives a clue in probing the emergent symmetry at a DQCP.

In conclusion, our numerical results unambiguously show a weakly first-order plaquette-AFM transition in the SS model. Though the ground state favors the EPL configuration, the FPL is energetically competitive, and can be stabilized as the ground state under a ring-exchange-like perturbation that preserves the SS lattice symmetry. Moreover, we provide evidence for a DQCP with an emergent $SO(5)$ symmetry at the triple point where the EPL, FPL, and AFM phases meet in the global phase diagram of the generalized SS model. Unusual topological excitations dictated by the emergent symmetry are expected and deserve detailed investigations.

Acknowledgments. We are thankful for fruitful discussions with Y. Cui, W. Ding, C. Liu, B. Normand, A. W. Sandvik, L. Wang, Y. Wang, W. Yu, and H. Zou. This work was supported by the National R&D Program of China (Grants No. 2017YFA0302900 and No. 2016YFA0300500), the National Natural Science Foundation of China (Grants No. 12174441, No. 12274458 and No. 11774420), and the Fundamental Research Funds for the Central Universities and the Research Funds of Renmin University of China (Grants No. 18XNLG24, No. 20XNLG19, and No. 23XNH081). Computational resources have been provided by the Physical Laboratory of High Performance Computing at Renmin University of China.

-
- [1] *Frustrated Spin Systems*, edited by H. T. Diep (World Scientific, Singapore, 2004).
- [2] *Introduction to Frustrated Magnetism, Materials, Experiments, Theory*, edited by C. Lacroix, P. Mendels, and F. Mila (Springer, Berlin, 2010).
- [3] L. Balents, Spin liquid in frustrated magnets, *Nature (London)* **464**, 199 (2010).
- [4] L. Savary and L. Balents, Quantum spin liquids: A review, *Rep. Prog. Phys.* **80**, 016502 (2017).
- [5] Y. Zhou, K. Kanoda, and T.-K. Ng, Quantum spin liquid states, *Rev. Mod. Phys.* **89**, 025003 (2017).
- [6] R. Yu and Q. Si, Antiferroquadrupolar and Ising-Nematic Orders of a Frustrated Bilinear-Biquadratic Heisenberg Model and Implications for the Magnetism of FeSe, *Phys. Rev. Lett.* **115**, 116401 (2015).
- [7] T. Senthil, A. Vishwanath, L. Balents, S. Sachdev, and M. P. A. Fisher, Deconfined quantum critical points, *Science* **303**, 1490 (2004).
- [8] T. Senthil, M. Vojta, and S. Sachdev, Weak magnetism and non-Fermi liquids near heavy-fermion critical points, *Phys. Rev. B* **69**, 035111 (2004).
- [9] Z. H. Liu, M. Vojta, F. F. Assaad, and L. Janssen, Metallic and Deconfined Quantum Criticality in Dirac Systems, *Phys. Rev. Lett.* **128**, 087201 (2022).
- [10] A. W. Sandvik, Evidence for Deconfined Quantum Criticality in a Two-Dimensional Heisenberg Model with Four-Spin Interactions, *Phys. Rev. Lett.* **98**, 227202 (2007).
- [11] N. Ma, G.-Y. Sun, Y.-Z. You, C. Xu, A. Vishwanath, A. W. Sandvik, and Z. Y. Meng, Dynamical signature of fractionalization at the deconfined quantum critical point, *Phys. Rev. B* **98**, 174421 (2018).
- [12] H. Shao, W. Guo, and A. W. Sandvik, Quantum criticality with two length scales, *Science* **352**, 213 (2016).
- [13] B. S. Shastry and B. Sutherland, Exact ground state of a quantum mechanical antiferromagnet, *Physica B+C* **108**, 1069 (1981).
- [14] A. Koga and N. Kawakami, Quantum Phase Transitions in the Shastry-Sutherland Model for $SrCu_2(BO_3)_2$, *Phys. Rev. Lett.* **84**, 4461 (2000).
- [15] C. H. Chung, J. B. Marston, and S. Sachdev, Quantum phases of the Shastry-Sutherland antiferromagnet: Application to $SrCu_2(BO_3)_2$, *Phys. Rev. B* **64**, 134407 (2001).
- [16] J. H. Pixley, R. Yu, and Q. Si, Quantum Phases of the Shastry-Sutherland Kondo Lattice: Implications for the Global Phase Diagram of Heavy-Fermion Metals, *Phys. Rev. Lett.* **113**, 176402 (2014).
- [17] P. Corboz and F. Mila, Tensor network study of the Shastry-Sutherland model in zero magnetic field, *Phys. Rev. B* **87**, 115144 (2013).
- [18] C. Boos, S. P. G. Crone, I. A. Niesen, P. Corboz, K. P. Schmidt, and F. Mila, Competition between intermediate plaquette phases in $SrCu_2(BO_3)_2$ under pressure, *Phys. Rev. B* **100**, 140413(R) (2019).
- [19] J. Y. Lee, Y. Z. You, S. Sachdev, and A. Vishwanath, Signatures of a Deconfined Phase Transition on the Shastry-Sutherland Lattice: Applications to Quantum Critical $SrCu_2(BO_3)_2$, *Phys. Rev. X* **9**, 041037 (2019).
- [20] J. Yang, A. W. Sandvik, and L. Wang, Quantum criticality and spin liquid phase in the Shastry-Sutherland model, *Phys. Rev. B* **105**, L060409 (2022).
- [21] K. Wierschem and P. Sengupta, Columnar Antiferromagnetic Order and Spin Supersolid Phase on the Extended

- Shastry-Sutherland Lattice, *Phys. Rev. Lett.* **110**, 207207 (2013).
- [22] H. Kageyama, K. Yoshimura, R. Stern, N. V. Mushnikov, K. Onizuka, M. Kato, K. Kosuge, C. P. Slichter, T. Goto, and Y. Ueda, Exact Dimer Ground State and Quantized Magnetization Plateaus in the Two-Dimensional Spin System $\text{SrCu}_2(\text{BO}_3)_2$, *Phys. Rev. Lett.* **82**, 3168 (1999).
- [23] S. Miyahara and K. Ueda, Exact Dimer Ground State of the Two Dimensional Heisenberg Spin System $\text{SrCu}_2(\text{BO}_3)_2$, *Phys. Rev. Lett.* **82**, 3701 (1999).
- [24] M. E. Zayed, Ch. Rüegg, J. Larrea J., A. M. Läuchli, C. Panagopoulos, S. S. Saxena, M. Ellerby, D. F. McMorrow, Th. Strässle, S. Klotz, G. Hamel, R. A. Sadykov, V. Pomjakushina, M. Boehm, M. Jiménez-Ruiz, A. Schneidewind, E. Pomjakushina, M. Stingaciu, K. Conder, and H. M. Rønnow, 4-spin plaquette singlet state in the Shastry-Sutherland compound $\text{SrCu}_2(\text{BO}_3)_2$, *Nat. Phys.* **13**, 962 (2017).
- [25] T. Waki, K. Arai, M. Takigawa, Y. Saiga, Y. Uwatoko, H. Kageyama, and Y. Ueda, A novel ordered phase in $\text{SrCu}_2(\text{BO}_3)_2$ under high pressure, *J. Phys. Soc. Jpn.* **76**, 073710 (2007).
- [26] S. Haravifard, D. Graf, A. E. Feiguin, C. D. Batista, J. C. Lang, D. M. Silevitch, G. Srajer, B. D. Gaulin, H. A. Dabkowska, and T. F. Rosenbaum, Crystallization of spin superlattices with pressure and field in the layered magnet $\text{SrCu}_2(\text{BO}_3)_2$, *Nat. Commun.* **7**, 11956 (2016).
- [27] S. Bettler, L. Stoppel, Z. Yan, S. Gvasaliya, and A. Zheludev, Sign switching of dimer correlations in $\text{SrCu}_2(\text{BO}_3)_2$ under hydrostatic pressure, *Phys. Rev. Res.* **2**, 012010(R) (2020).
- [28] J. Guo, G. Sun, B. Zhao, L. Wang, W. Hong, V. A. Sidorov, N. Ma, Q. Wu, S. Li, Z.-Y. Meng, A. W. Sandvik, and L. Sun, Quantum Phases of $\text{SrCu}_2(\text{BO}_3)_2$ from High-Pressure Thermodynamics, *Phys. Rev. Lett.* **124**, 206602 (2020).
- [29] J. Larrea Jiménez, S. P. G. Crone, E. Fogh, M. E. Zayed, R. Lortz, E. Pomjakushina, K. Conder, A. M. Läuchli, L. Weber, S. Wessel, A. Honecker, B. Normand, Ch. Rüegg, P. Corboz, H. M. Rønnow, and F. Mila, A quantum magnetic analogue to the critical point of water, *Nature (London)* **592**, 370 (2021).
- [30] Y. Cui, L. Liu, H. Lin, K.-H. Wu, W. Hong, X. Liu, C. Li, Z. Hu, N. Xi, S. Li, R. Yu, A. W. Sandvik, and W. Yu, Proximate deconfined quantum critical point in $\text{SrCu}_2(\text{BO}_3)_2$, *Science* **380**, 1179 (2023).
- [31] See Supplemental Material at <http://link.aps.org/supplemental/10.1103/PhysRevB.107.L220408> for details about the variational optimization and fitting and extrapolation, which includes Refs. [14,17,20,32–37,39–41,43,44,52].
- [32] Z. Y. Xie, J. Chen, J. F. Yu, X. Kong, B. Normand, and T. Xiang, Tensor Renormalization of Quantum Many-Body Systems Using Projected Entangled Simplex States, *Phys. Rev. X* **4**, 011025 (2014).
- [33] H. J. Liao, Z. Y. Xie, J. Chen, Z. Y. Liu, H. D. Xie, R. Z. Huang, B. Normand, and T. Xiang, Gapless Spin-Liquid Ground State in the $S = 1/2$ Kagome Antiferromagnet, *Phys. Rev. Lett.* **118**, 137202 (2017).
- [34] H.-J. Liao, J.-G. Liu, L. Wang, and T. Xiang, Differentiable Programming Tensor Networks, *Phys. Rev. X* **9**, 031041 (2019).
- [35] B.-B. Chen, Y. Gao, Y.-B. Guo, Y. Liu, H.-H. Zhao, H.-J. Liao, L. Wang, T. Xiang, W. Li, and Z. Y. Xie, Automatic differentiation for second renormalization of tensor networks, *Phys. Rev. B* **101**, 220409(R) (2020).
- [36] B. Ponsioen, F. F. Assaad, and P. Corboz, Automatic differentiation applied to excitations with projected entangled pair states, *SciPost Phys.* **12**, 006 (2022).
- [37] H. C. Jiang, Z. Y. Weng, and T. Xiang, Accurate Determination of Tensor Network State of Quantum Lattice Models in Two Dimensions, *Phys. Rev. Lett.* **101**, 090603 (2008).
- [38] P. Corboz, T. M. Rice, and M. Troyer, Competing States in the t - J model: Uniform D -Wave State Versus Stripe State, *Phys. Rev. Lett.* **113**, 046402 (2014).
- [39] H. N. Phien, J. A. Bengua, H. D. Tuan, P. Corboz, and R. Orús, Infinite projected entangled pair states algorithm improved: Fast full update and gauge fixing, *Phys. Rev. B* **92**, 035142 (2015).
- [40] P. Corboz, Variational optimization with infinite projected entangled-pair states, *Phys. Rev. B* **94**, 035133 (2016).
- [41] L. Wang and F. Verstraete, Cluster update for tensor network states, [arXiv:1110.4362](https://arxiv.org/abs/1110.4362).
- [42] X. F. Liu, Y. F. Fu, W. Q. Yu, J. F. Yu, and Z. Y. Xie, Variational corner transfer matrix renormalization group method for classical statistical models, *Chin. Phys. Lett.* **39**, 067502 (2022).
- [43] Zygote package, <https://fluxml.ai/Zygote.jl/dev/>.
- [44] F. Verstraete and J. I. Cirac, Renormalization algorithms for quantum-many body systems in two and higher dimensions, [arXiv:cond-mat/0407066](https://arxiv.org/abs/cond-mat/0407066).
- [45] B. Zhao, P. Weinberg, and A. W. Sandvik, Symmetry-enhanced discontinuous phase transition in a two-dimensional quantum magnet, *Nat. Phys.* **15**, 678 (2019).
- [46] W.-Y. Liu, S.-S. Gong, Y.-B. Li, D. Poilblanc, W.-Q. Chen, and Z.-C. Gu, Gapless quantum spin liquid and global phase diagram of the spin-1/2 J_1 - J_2 square antiferromagnetic Heisenberg model, *Sci. Bull.* **67**, 1034 (2022).
- [47] L. Wang and A. W. Sandvik, Critical Level Crossings and Gapless Spin Liquid in the Square-Lattice Spin-1/2 J_1 - J_2 Heisenberg Antiferromagnet, *Phys. Rev. Lett.* **121**, 107202 (2018).
- [48] W. Brenig and A. Honecker, Planar pyrochlore: A strong-coupling analysis, *Phys. Rev. B* **65**, 140407(R) (2002).
- [49] J.-B. Fouet, M. Mambrini, P. Sindzingre, and C. Lhuillier, Planar pyrochlore: A valence-bond crystal, *Phys. Rev. B* **67**, 054411 (2003).
- [50] E. Berg, E. Altman, and A. Auerbach, Singlet Excitations in Pyrochlore: A Study of Quantum Frustration, *Phys. Rev. Lett.* **90**, 147204 (2003).
- [51] H. Zou, F. Yang, and W. Ku, Nearly degenerate ground states of a checkerboard antiferromagnet and their bosonic interpretation, [arXiv:2011.06520](https://arxiv.org/abs/2011.06520).
- [52] A. W. Sandvik and H. G. Evertz, Loop updates for variational and projector quantum Monte Carlo simulations in the valence-bond basis, *Phys. Rev. B* **82**, 024407 (2010).